Microscopic Imaging of Epigenetic Age.

Delany Rodriguez[1], Lorenzo Fiengo[1], Martin Alvarez-Kuglen[1], Haodong Qin [2], Chen Farhy[1], Aaron Havas[1], Rozalyn M. Anderson[3], Peter D. Adams[1], Tatyana O. Sharpee[2], and Alexey V. Terskikh[1*]
1. Sanford Burnham Prebys, La Jolla CA 92037.
2. Salk Institute for Biological Studies, La Jolla, CA 92037, USA
3. University of Wisconsin, Madison, WI 53705, USA
* Correspondence: terskikh@sbp.edu

ABSTRACT.
Predictive biomarkers of functional or biological age are key for evaluating interventions aimed at increasing healthspan and / or lifespan in humans. Currently, cardiovascular performance, blood analytes, frailty indices, and DNA methylation clocks are used to provide such estimates; each technique has its own challenges and limitations. We have developed a novel approach, microscopic imaging of biological age (miBioAge), which computes multiparametric signatures based on the patterns of epigenetic landscape in single nuclei. We demonstrated that such miBioAge readouts can robustly distinguish young and old cells from multiple tissues, reveal aging progression in peripheral blood (e.g. CD3+ T cells), and reflect changes of epigenetic signatures consistent with expected slowdown or acceleration of biological age in chronologically identical mice treated with caloric restriction or chemotherapy. Because miBioAge readouts are computed from individual samples without applying linear regression, we posit that this novel biomarker may provide personalized assessment of functional aging.

INTRODUCTION.
Studies in animals and humans have identified several interconnected processes associated with aging [1] which promote tissue specific epigenetic changes [2]. One of the best studied, H3K9me3, marks constitutive heterochromatin [3]. Both H3K27me3 and H4K20me3 marks are associated with promoters of repressed genes [4]. H3K27me3 represses many genes involved in development and stem cell differentiation [5]. H4K20me3 plays a role in silencing of repetitive DNA and transposons [6] and functions to suppress cell senescence and tumorigenesis [7]. Further, the pattern of active enhancers, marked with a combination of H3K27ac & H3K4me1 [8], is clearly age-dependent both in terminally differentiated cells (e.g. CD8+ T cells [9]) and residents somatic stem cells (e.g. neural stem cells [10]). Many other histone modifications and epigenetic mechanisms were linked to aging and longevity [11].

However, the best quantified age-associated epigenetic changes in the past decade are the changes of DNA methylation. Fascinating discoveries of Hannum et al., [12] and Horvath et al., [13] identified CpG sites in human blood and other tissues with age-dependent changes in DNA methylation enabling the development of epigenetic clocks; subsequently, multiple other combinations of CpGs / clocks have been established for various mammals [14] using blood cells as well as other tissues [12, 15-17]. All DNA methylation clocks depend on linear regression algorithms or deep learning [18] to select CpGs methylation sites with levels that best fit chronological age resulting in rather accurate chronological clocks tailored to specific cell types or pan tissues [19]. The manifestations of aging vary dramatically among individuals of the same chronological age, bringing forth the notion of biological age which can be estimated using candidate biomarkers including cardiovascular performance, serum analytes, epigenetic markers, and deficit or frailty indices [20]. For DNA methylation clocks the deviation from the linear regression prediction of chronological age for each individual is considered a measure of biological age. Based on several hundreds of thousands of thousands of which might be individual specific and biologically relevant CpGs which may track with individual organismal or tissue function or biological age rather than chronological age [21]. PhenoAge [22] and GrimAge [16] clocks attempt to

overcome this limitation through alternative training approaches by including additional CpGs regressed on empirically observed plasma proteins whose levels serve as surrogate biomarkers previously correlated with healthspan and lifespan. Despite all adjustments these clocks remain population level predictors rather than personalized instruments. Further, DNA methylation clocks are dependent on the particular method of calibration [23], often require large number of cells, and are not cost effective [19], underscoring the need for developing of alternative approaches to measure functional or biological age.

Several years ago, we developed a novel screening approach, microscopic imaging of epigenetic landscapes, which is rooted in the analysis of epigenome topography in single nuclei of intact permeabilized cells [24]. We used immunolabeling with antibodies specific for histone modifications (e.g. acetylation and methylation marks), then visualized nuclear staining of these marks using automated microscopy and captured patterns using image texture analysis, resulting in a multiparametric signatures of cellular states. This approach enabled us to distinguish different cell types, discriminate classes of epigenetically active drugs, and identify signatures of primary human differentiated glioblastoma cells [24].

Here we took advantage of this technique to study aging and described a novel candidate biomarker of functional aging - microscopic imaging of biological age (miBioAge). We demonstrated that miBioAge successfully distinguished cells from chronologically young and old mice and humans in all tissues and organs analyzed. Further, miBioAge readouts of peripheral blood mononuclear cells (PBMC) and the CD3+ T cells correlated with chronological age without any manipulation of the underlying multiparametric signatures (e.g. no linear regression selecting for chronological age), suggestingsuggesting that unselected miBioAge provides a readout of individual epigenetic state in each cell which is related to the functional age. Finally, miBioAge faithfully detected the acceleration of epigenetic aging after Doxorubicin (DOX) treatment and slowdown of epigenetic aging following Caloric Restriction (CR) diet, suggesting that miBioAge reflects biological age.

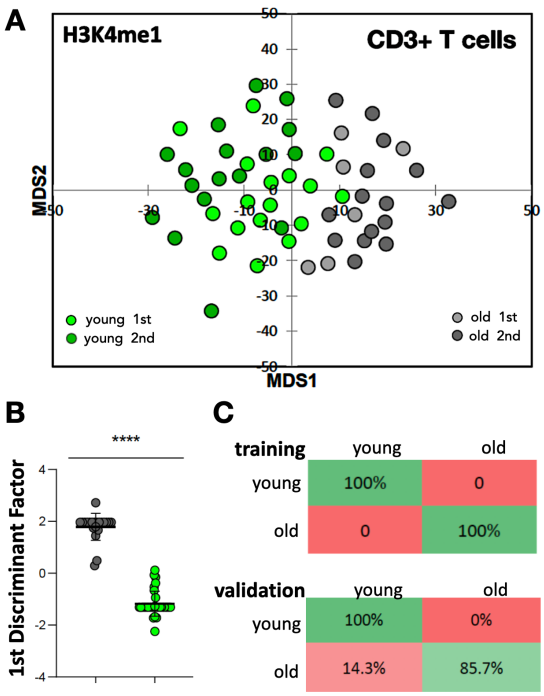

Fig. 1. Multiparametric signatures based on H3K4me1 mark (+DAPI) separates single CD3+ cells from young and old mice. (**A**) Multidimensional Scaling (MDS) plot of single CD3+ cells from 2 young and 2 old mice. (**B, C**) Quadratic discriminant analysis (QDA) using texture features derived from images obtained with anti-H3K4me1 + DAPI quantifies the separation between young vs old cell. (B) Scatter plot showing first discriminant factor (F1), **** p<0.0001 t-test; (C) confusion matrixes showing accuracy (percentage) of correct predictions for the training and validation sets.

RESULTS.

Multiparametric signatures distinguish young and old CD3+ subset of PBMC

We inquired whether multiparametric epigenetic signatures [24] could detect age-dependent epigenetic changes distinguishing cells from young and old mice. We first analyzed CD3+ subset of mouse PBMC immunolabeled with anti-H3K4me1and anti-CD3 (+DAPI) and multiparametric signatures were computed (see Materials and Methods for details). We observed a clear separation between young and old cells using multidimensional scaling (MDS) algorithm implemented in XLSTAT software (**Fig. 1A**). Further, individual CD3+ cells from young and old mice were readily discriminated with 85.7% accuracy using quadratic discriminant analysis (QDA) (**Fig. 1B, C**). These results suggest that multiparametric

signatures of epigenetic landscape in single cells are sufficient to distinguish young and old CD3+ cells with high accuracy.

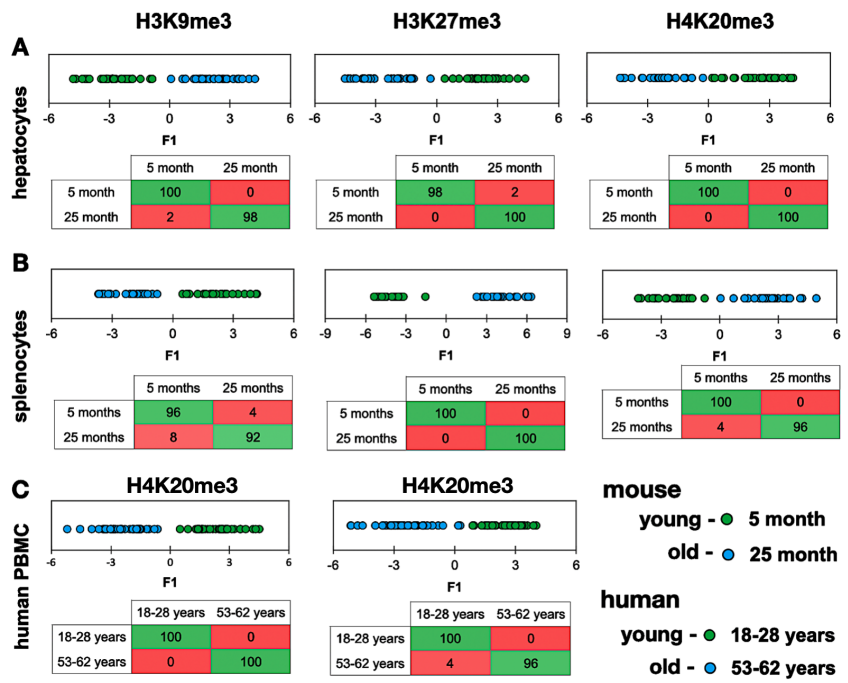

Fig. 2. QDA analysis discriminates young vs old cells. Quadratic discriminant analysis using texture features derived from images obtained using antibodies to H3K9me3, H3K27me3, H4K20me3 (columns) was used to separate (**A**) mouse hepatocytes (**B**) mouse splenocytes, (**C**) human PBMC. Top rows, scatter plot showing first discriminant factor (F1), lower rows, confusion matrixes showing accuracy (percentage) of correct predictions for the validation set; larger numbers (and green color coding) suggest better prediction.

Multiparametric signatures distinguish young and old freshly isolated cells of different types.

Based on availability and ease of harvesting we focused on freshly isolated hepatocytes and splenocytes from 5 months or 25 months old C57BL/6J males. Hepatocytes were purified via a 2-step perfusion method modified from [25] resulting in ~98% pure viable primary hepatocytes. Cells were fixed, immunolabeled (separately) with anti-H3K9me3, anti-H3K27me3, or anti-H4K20me3 (+DAPI), and multiparametric signatures were computed. We discovered that multiparametric signatures based on any of the above epigenetic mark robustly (92-100% accuracy) discriminated between young and old hepatocytes as well as young and old splenocytes (**Fig. 2A, B).** Further, we analyzed de-identified "young" (18-28 years old) and "old" (53-62 years old) normal human peripheral blood mononuclear cells (PBMC) obtained from a commercial source. We discovered a robust (96-100% accuracy) separation between the young and the old primary human PBMC (**Fig. 2C**). These results suggest that multiparametric epigenetic signatures based on well-characterized epigenetic marks of heterochromatin can discriminate between young and old freshly isolated mouse and human cells.

Linear regression of multiparametric epigenetic signatures provides excellent chronological clock.

Next, we inquired whether multiparametric epigenetic signatures could be regressed onto chronological age. We obtained mouse PBMC ranging from 53 to 968 days from C57BL/6J males using classical Ficoll centrifugation procedure. Cells were fixed, immunolabelled with anti-H3K4me1, anti-CD3 (+DAPI) and multiparametric signatures were computed. We employed classical linear regression analysis implemented in XLSTAT package (Base, v19.06) to select features with the best prediction power/correlation with chronological age. We observed an excellent (r=0.96, RMSE= 66, p=1.9e-9 for the validation set) correlation of the regressed features with chronological age (**Fig. 3A**). The residuals were normally distributed and centered similarly to the training set, validating an assumption a normal distribution. To avoid the artifacts of cellularity change with age (e.g. increased myeloid and decreased lymphoid representation) we have analyzed only the CD3+ cells representing a total T cell compartment. Similar to that observed for PBMC, we detected a very good (r=0.95, RMSE=99, p=2.9e-16 for the validation set) correlation of the regressed features with chronological age for the CD3+ cells (**Fig. 3B**). Quadratic discriminant analysis using linear regression-adjusted signatures of young

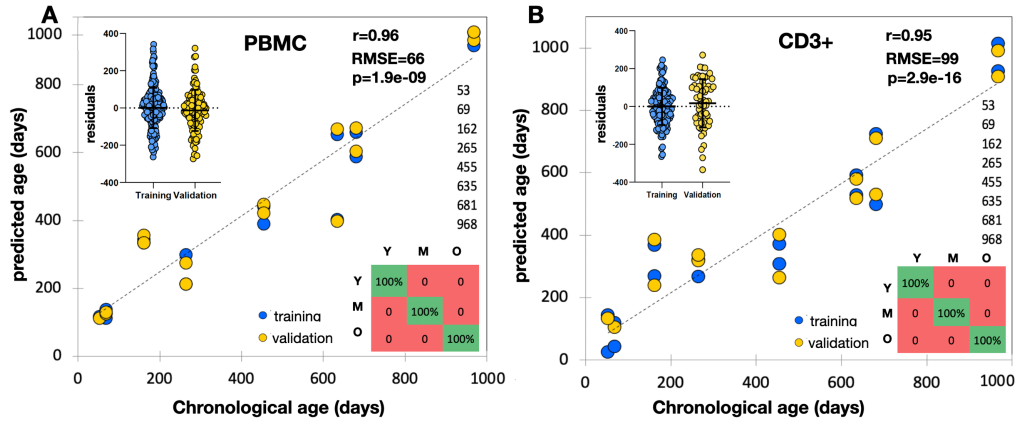

Fig. 3. Linearly regressed multiparametric epigenetic signatures correlate with chronological age. Dot plots of linear regression analysis for training and validation sets using PBMC or CD3 T cell subset multiparametric signatures based on H3K4me1 (+DAPI). Each dot is individual animal. Inserts in the left top corner, residuals distribution using 10 technical replicates per each mouse to better visualize the distribution. Insert in the right lower corner, quadratic discriminant analyses confusion matrix based on the validation set accurately (100%) separates signatures of young (Y) vs middle age (M) vs old (M) PBMC and CD3+ T cells.). r, Person correlation coefficient. RMSE, root mean square error, p, statistical significance of Pearson correlation. Regression trendline is shown for the validation set. Computations with Xlstat package (Base, v19.06).

(53-69 days), middle age (162-455 days), and old (632-968 days) mice separated all three groups with 100% accuracy for both PBMC and CD3+ T cells. These results argue for the utility of H4K20me3-based epigenetic signatures to measure chronological age in mouse PBMC and CD3+ T cells. Given the power of MIEL to discriminate between other types of young and old cells including human PBMC, we predict the utility of chronological miBioAge for many other cell types of mice and men.

Aging trajectories of epigenetic signatures support the notion of miBioAge axis

Next, we investigated the trajectories of epigenetic signatures with respect to age without the assumption of linear progression or trajectory and without applying linear regression (or any other feature transformation) of the texture features space. To that end we computed the coordinates of centroids of all datapoints from youngest and oldest mice in the multidimensional space. Subsequently we computed the distances from each datapoint (all ages) to the centroids of the youngest and oldest mice enabling us to plot each datapoint in such coordinates (**Fig. 4A, B**). We observed a distribution of data points from youngest to oldest mice around

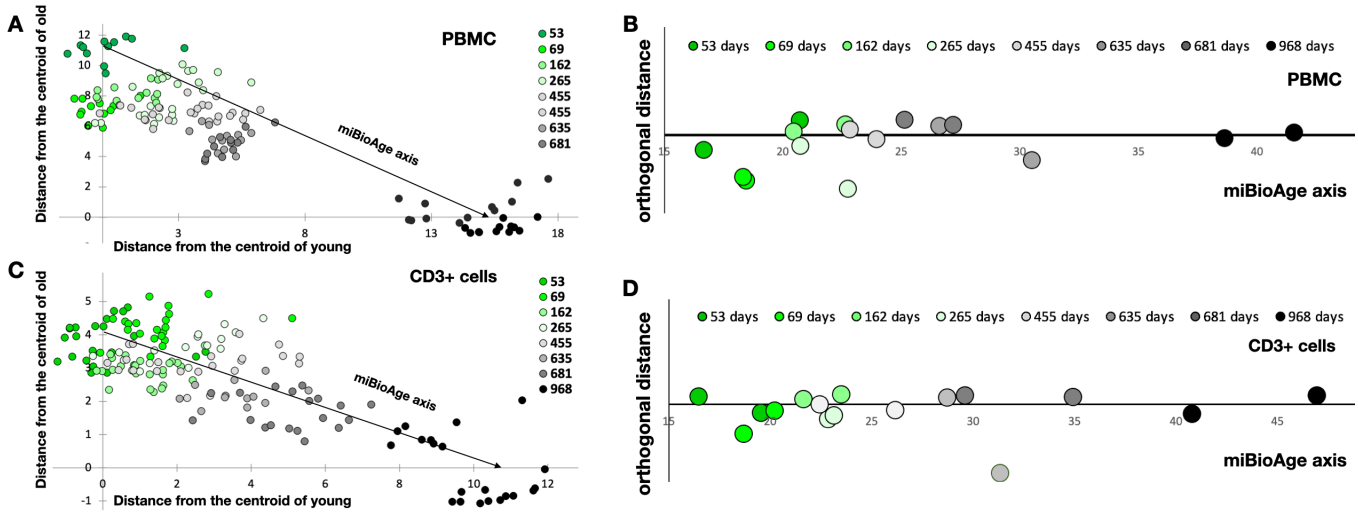

Fig. 4. Defining miBioAge axis. (**A, C**) Dot plots of the distance from the centroids of youngest mice (X axis) and the distance from the centroids of oldest mice (Y axis). Each point is a technical replicate (well mean, n=12 / mouse, ~3000 cells / replicate). Mouse ages (days) are color coded. Solid line connecting the centroids of the oldest mice to the centroids of the youngest mice visualizing the miBioAge axis. (**B, D**) Centroids of individual mice from A and B plotted in miBioAge and orthogonal (orthogonal distance to miBioAge axis) coordinates.

the respective centroids with intermediate aged datapoints falling in-between the youngest and oldest mice for both PBMC and CD3+ cells (**Fig. 4A, B**).

These results suggested an apparent age-related distribution (or progression) of epigenetic signatures along a linear trajectory between the youngest and the oldest mice. Therefore, we designed a new axis connecting the centroids of the youngest and oldest mice signatures hereon referred to as the "miBioAge axis." The progression of each replicate was evaluated by projecting onto the miBoAge axis. In addition, we considered distance perpendicular miBioAge axis as "orthogonal distance" axis (**Fig. 4B, D)**. Note that all distances and projections should be first computed in the multidimensional Euclidean space and the results are then plotted in 2D space as miBioAge vs orthogonal distance. The miBioAge axis now provides a simple readout of the proximity to the oldest / youngest centroids and the orthogonal axis estimates the deviation from the "perfect" epigenetic age trajectory along miBioAge axis. Note, that the position of each mouse on miBioAge axis is a mere projection of its entire multiparametric signature without linear regression or any other manipulations.

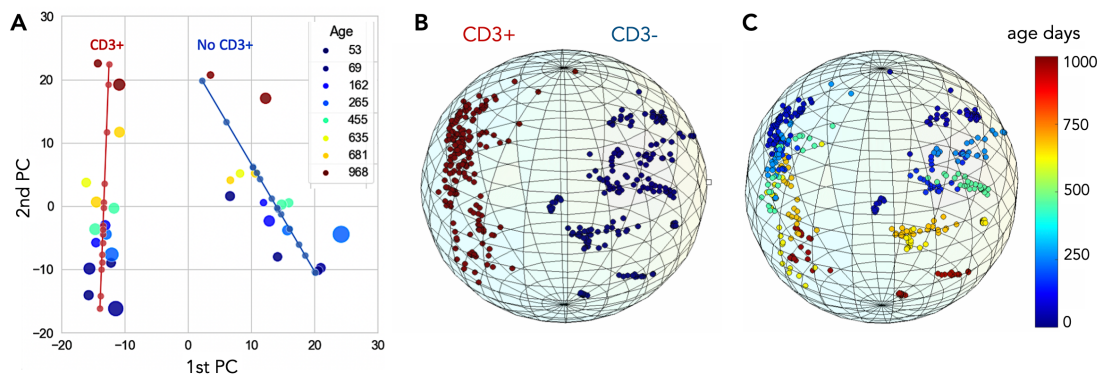

Fig. 5. Alternative analysis of age-dependent progression of epigenetic signatures. A. Euclidian PCA separates datapoint by cell type CD3+ vs CD3- (PC1) and separation of datapoints within each lineage by age (PC2). Each dot is a centroid of a mouse. **B.** A 3-dimantrional hyperbolic embedding separates CD3+ and CD3- subsets of PBMC. Each dot is a technical replicate (well mean, n=12 / mouse, ~3000 cells / replicate) **C.** Same 3-dimentional hyperbolic embedding as in (B), but the datapoints are colored by age to reveal the emergence of the aging trajectories. Movies of B and C are available upon request.

Alternative computational techniques extract intrinsic aging trajectories

To pressure test the emerging age-related progression of epigenetic signatures projected on the miBoAge axis, we employed a straightforward Principal Component Analysis (PCA). We compared complimentary subpopulations of PBMC, namely CD3+ and CD3- cells. PCA revealed a clear separation of datapoint by cell type CD3+ vs CD3- (mainly by PC1) and progression of age-related multiparametric signatures within each lineage (mainly by PC2) (**Fig. 5A**). Note that axis of the age separation in CD3+ population is nearly parallel to PC2, hence, in this case PC2 is similar to the miBioAge axis for CD3+ cells.

Further, to explore yet another alternative route of analysis we took advantage of the Hyperbolic space recently proven to be particularly helpful to analyze complex biological datasets [26-29]. We optimized the dimensionality and the curvature for data embedding as previously described [26, 27] (see Materials and Methods for detailed description of Hyperbolic embedding). Remarkably, similar to PCA results, we observed a clear separation of signatures between CD3+ and CD3- cells in a 3D hyperbolic space (**Fig. 5B)** and the emergence of age-related progression of multiparametric signatures for both CD3+ and CD3- subsets of PBMCs (**Fig. 5D**).

Taken together, these results strongly suggest the presence of intrinsic aging trajectories within epigenetic signatures of mouse PBMCs and CD3+/- subsets. Note that none of the methods described above require

linear regression or any other manipulation of texture feature values to extract the progression of multiparametric signatures along the aging axis.

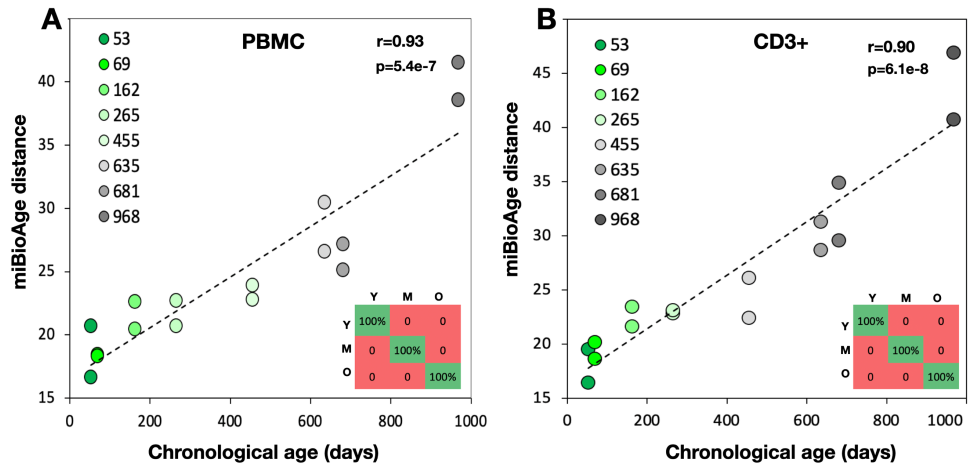

Fig. 6. miBioAge readouts correlate with chronological age. Dot plot of miBioAge readouts vs chronological age. Native multiparametric signatures based on H3K4me1 (+DAPI) were used without linear regression. Each dot is individual animals. Insert in the right lower corner, quadratic discriminant analyses confusion matrix based on the validation set accurately (100%) separates signatures of young (Y) vs middle age (M) vs old (M) PBMC and CD3+ T cells.). r, Person correlation coefficient. RMSE, root mean square error, p, statistical significance of Pearson correlation. Trendline is shown for visualization only. Computations with XLSTAT package (Base, v19.06).

miBioAge correlates with chronological age

Intrigued by an intrinsic age-associated progression of epigenic miBioAge readouts we plotted miBioAge readouts vs chronological age. Remarkably, we observe a rather good (r=0.93, PBMC and r=0.90, CD3+ cells) correlation with chronological age (**Fig. 6C, D**), albeit lower compared to the model based on linear regression (**Fig. 3**). Similar to that observed for the linear regression model, quadratic discriminant analysis using unmanipulated multiparametric signatures of young (53-69 days), middle age (162-455 days), and old (632-968 days) mice separated all three groups with 100% accuracy for both PBMC and CD3+ T cell. The limited numbers of mice (16 total) precluded us from obtaining more refined statistics.

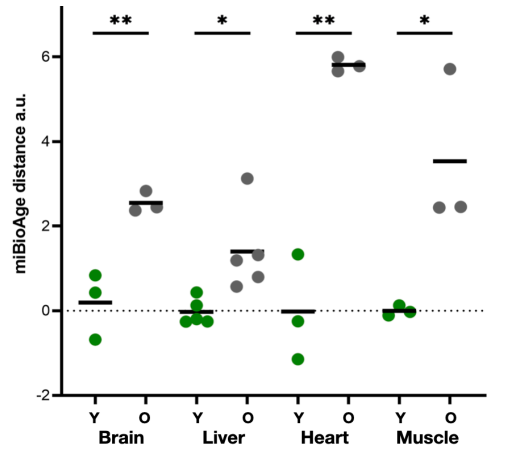

Fig. 7. miBioAge distinguishes young and old nuclei from solid organs and tissues. Dot plot of miBioAge readouts of young and old nuclei of corresponding tissues. Y=young (2 mo) and O=old (27 mo). The multiparametric signatures are based on H3K27me3 + H3K27ac marks (+DAPI). Each dot represents an individual mouse. *p<0.05, **p<0.01, 2-tailed unpaired t-test.

miBioAge separates young and old nuclei from solid organs

Flash-frozen in liquid nitrogen (stored at -80°C) is a common practice to preserve tissue and organs that are not to be processed immediately [30-32]. To test if we could extract epigenetic signatures from flash-frozen tissues, we developed a protocol that allowed us to isolate nuclei and then perform the analysis of epigenetic landscape similar to that described in freshly fixed cells (see Materials and Methods). We isolated nuclei from frozen brain, liver, heart, skeletal muscle (quadriceps) of young (2 mo) and old (27 mo) mice and immunolabeled them with anti-H3K27me3 and anti-H3K27ac (+DAPI) and computed multiparametric signatures. Similar to that observed in freshly fixed cells, miBioAge readouts discriminated samples from young and old mice in all tissues analyzed (**Fig. 7**). Curiously, miBioAge distances of young and old centroids vary between organs: 2.6 for brain, 1.3 for liver, 5.8 for heart, and 3.5 for skeletal muscles (**Fig. 7**). These results suggest that we can extract multiparametric epigenetic signatures from flash-frozen tissues allowing us to ultimately analyze samples at later stages and/or use samples from collaborators.

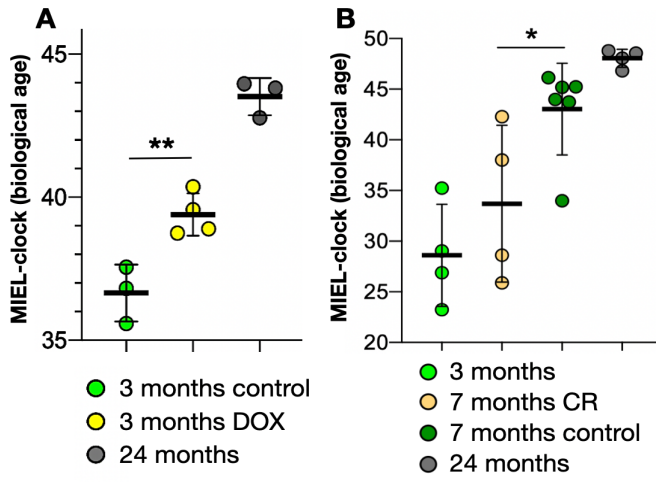

Fig. 8. miBioAge detects epigenetic alterations induced by DOX and CR. Dot plot comparing miBioAge readouts based on H3K27me3 + H3K27ac marks (+DAPI). of **A.** liver hepatocytes isolated from DOX-treated (21 days), untreated controls, and old mice **B.** liver nuclei isolated from CR mice (5 months 25% CR), controls, and old mice. *=p<0.05, **=p<0.001, one-way ANOVA with Tukey's post hoc.

miBioAge distinguishes experimental perturbation affecting biological age

Previous work from the Campisi laboratory [33] and others [34-36] demonstrated the age-accelerating effect of widely used chemotherapeutic agents. We followed Demaria et al., 2017 [33] protocol for DOX treatment (10 mg/kg, i.p.; controls received PBS). Live hepatocytes were isolated 21 days post injection using a 2-step perfusion method modified from [25] resulting in ~98% pure viable primary hepatocytes. Day 21 post DOX treatment was chosen to focus on aging-related changes as opposed to acute response to DNA damage and stress response. Hepatocytes were plated in 384 well plates, fixed, immunolabelled with anti-H3K9me3 and anti-H3K27ac (+DAPI), and multiparametric signatures were computed. We observed that DOX treatment shifted the miBioAge readouts from freshly isolated liver hepatocytes towards that of an older age (**Fig. 4A**).

Multiple studies suggest that CR slows down aging in diverse species [37-39]. Frozen liver samples from CR and control mice were obtained from Rozalyn Anderson (University of Wisconsin). Nuclei were purified from frozen liver tissues as previously described [40], plates in 384 well plates, fixed, immunolabelled with anti-H3K9me3 and anti-H3K27ac (+DAPI), and multiparametric signatures were computed. CR treatment shifts the miBioAge signatures in liver hepatocytes towards the younger age (**Fig. 4B**). These observations suggest that unmanipulated miBioAge signatures of liver hepatocytes readily discriminate experimental perturbation of biological age.

DISCUSSION.

One of our most surprising findings is the discovery of intrinsic aging trajectories within multiparametric epigenetic signatures of mouse PBMCs and CD3+/- subsets that could be rendered and visualized using both Euclidian and hyperbolic metrics. Remarkably, this approach does not require linear regression or any other manipulation of multiparametric texture features to extract the age-related progression of multiparametric signatures along the aging trajectory. We take it as a hint that unmanipulated multiparametric signatures may provide better estimation of biological differences between the animals. Our observations suggest the presence of an intrinsic age-related order in the multidimensional space of texture features, perhaps reflecting the robust spatial organization of 3-dimensional epigenetic landscapes in single nuclei and its evolution with age. It will be informative to further elucidate the structure of the feature space and the relationships between texture features obtained from imaging different epigenetic marks. Further, it would be revealing to compare the aging trajectories obtained from multiparametric signatures of different epigenetic marks and their combinations to determine whether the signatures of all marks change with age, what are the rates of age-related change for each mark, and whether combinatorial analysis could provide additional insights. The availability of specific and sustainable antibodies to dozens of epigenetic marks is likely to be the major limitation moving in that direction.

The aging process is associated with functional interconnected decline across multiple organs therefore impacting the health of the entire organism; the decline of one organ can promote the dysfunction of the entire organism accelerating the aging process [41]. Several studies suggest that organs and tissues age at a different rate. Transcriptomic analysis in mice [42] has demonstrated that organs show an inter- and intra-organ progression of aging. A differential gene expression analysis of 17 organs (including brain, heart, skeletal muscle, kidney) across multiple ages (and sex) identified gene sets that were expressed analogously in these organs yet differed in age onset. Perhaps not surprisingly, the most common differentially expressed genes across organs were related to immune response [42, 43]. Several studies identified diverse set of aging profiles termed ageotypes [44-46]. Even though there are similarities at the gene expression level, when individuals are grouped by ageotypes most of them show changes in immune ageotype correlated with liver and kidney dysfunction pathways, yet a few individuals showed the opposite trend. These and other studies support the idea that individual organs and tissues age at different rates, through different mechanisms that can influence the crosstalk between organs and ultimately the entire body [41, 44]. We observed a robust separation of young and old epigenetic signatures in all tissues and samples analyzed. Curiously, the miBioAge distances between young and old samples very significantly between tissues and organs perhaps reflecting the intrinsic differences in their pace of functional aging. However, further analysis is required to determine the weights of the texture features that provide discrimination between the young and the old signature in each organ in order to compare the aging rates across tissues and organs.

It appears that different cancers and cancer treatments induce epigenetic changes therefore increasing genome instability and accelerating the pace of organismal aging [47-51]. In particular, DNA damage (especially at a high rate) is known to induce cancer and accelerate aging [52-54] suggesting that, paradoxically, chemotherapy while suppressing an actively growing tumor, may promote delayed onset of neoplastic transformations. Most chemotherapy treatments have damaging effects to the entire organism and accelerate the aging process [33, 55-57]. It has been noted that cancer survivors develop age-related conditions faster (compared to healthy people) including increased frailty, chronic organ dysfunction, increase of cardiovascular diseases, cognitive impairment and secondary cancers [35, 58-61]. We observed a shift of miBioAge readouts towards that of the old animals in mice treated with Doxorubicin, resembling the observations in humans [36]. Cancer treatments vary wildly from surgery to chemotherapy to radiation and immunotherapy amongst others, all with the primary goal to eradicate cancer cells. Chemotherapy drugs, administered in the bloodstream, target cells at different phases of the cell cycle; doxorubicin causes damage to DNA and also blocks Topoisomerase II therefore preventing the cells from completing cell cycle [62, 63]. It will be important to investigate whether miBioAge readouts could faithfully report the effects of other chemotherapy drugs, evaluate different doses, regimens, and duration of treatment in various tissues. Quantitating the age acceleration following chemotherapy may help fine tuning and tailoring chemo regimens, quantify the utility of proposed dietary approaches that increase the resilience to chemotherapy [64], and possibly design new interventions aimed to reduce or eliminate accelerated aging following chemotherapy.

Because CR robustly increases maximum lifespan and delays biological aging in diverse scenarios [37-39], albeit the full picture could be more complex [65, 66]. successfully applied CR regimens help understanding the biology of aging [67-69] and could help recovery after chemotherapy in clinic [64]. We have observed a shift in miBioAge readouts in CR animals towards that of young animals consistent with the phenotypic observations. It will be important to further refine these analyses, covering different CR regimens in mice and other species (e.g. monkeys), and to correlate the epigenetic changes with functional readouts at the organismal level as well as with various OMICs datasets (e.g. gene expression, chromatin accessibility, and enrichment for various epigenetic marks).

Growing evidence suggest that epigenetic landscape controls gene transcription including a direct control at the promoter regions [70]. Multiple histone post-translational modifications (i.e., lysine acetylation, lysine methylation, arginine acetylation, arginine methylation, serine phosphorylation, lysine ubiquitination, amongst many others) govern nucleosome states and modify histone-DNA interactions [71]. The combinatorial effect of histone modifications (known as the histone code hypothesis) is thought to define functional states of the chromatin [72-74]. For instance, a cooperative action of multiple histone modifications can increase the robustness of transcriptional repression [4, 75]. We employed several common histone methylation and acetylation marks to determined multiparametric epigenetic signatures and have demonstrated their utility. However, systematic comparative analysis of these and many other marks across multiple tissues is a daunting task reserved for future studies. Investigation combinatorial complexity of epigenic marks represents formidable challenge. Our imaging approach was designed to be high throughput (e.g. compatible with 1536 well format), which makes it entirely possible to access hundreds of thousands of data points in a time and cost effective manner.

Since their discovery almost a decade ago, DNA methylation clocks have gained major grounds and have been widely explored in different areas of biological and medical studies [76-78]. It will be important to directly compare and contrast the DNA methylation clocks and miBioAge readouts. Whereas we anticipate an overall concordance of the two approaches, the differences are likely to emerge based on the underlying methodologies. The DNA methylation clocks have high DNA region-specific resolution capable of pinpointing the exact locations of selected CpGs islands. Although individual CpGs usually have low weights, collectively, their enrichment in particular areas of genome (e.g. enhancer regions [79]) may inform on the molecular mechanisms of underlying age-related changes. Detecting the exact chromatin regions responsible for any given multiparametric signature of the imaged nuclei will be challenging. However, miBioAge readouts could be more sensitive to functional differences at the individual organism level. Several DNAm clocks (e.g. PhenoAge [22], GrimAge [16], and meta-clock [80]) were trained to track with multiple age-related diseases. It will be important to explore whether miBioAge readouts could faithfully detect different disease states and conditions.

LIMITATIONS OF THE CURRENT STUDY.

The current study has several limitations. We will update this manuscript as the progress being made to address the following issues: The cellular composition of PBMC is changing with age and the frequency of CD3+ T cell subtypes is changing with age as well. For instance, young and old animals have various proportions of circulating naïve vs memory T cells, which may have distinct epigenetic landscape. A more refined subset of PBMCs needs to be analyzed across extended age groups. We have examined only of limited number of epigenetic marks and have not yet address their true combinatorial complexity, which is the key feature of epigenetic code. The 2-dimentional maximum projection of 3-dimentional nuclei inevitably degrade the information content, stressing the need to develop 3-dimentional approaches to volume texture analysis. Known variability and vulnerability related to isolating the intact unperturbed nucelli from flash frozen tissues could affect our results.

MATERIALS AND METHODS.

Mice

Experiments were conducted according to guidelines and protocols approved by the Institutional Animal Care and Use Committee (IACUC) of Sanford Burnham Prebys Medical Discovery Institute. Data presented within this manuscript were obtained using male mice. C57BL/6 mice, ranging in age from 2 to 27 months old, and were obtained from National Institute on Aging, Aged Rodent Colonies (RRID:SCR_007317).

Isolating Nuclei from Frozen Tissues

Organs and tissues were collected from mice and immediately snap frozen using liquid Nitrogen and stored at – 80°C. Organs and tissues were then transferred to a pre-chilled mortar and laid on top of dry ice; liquid Nitrogen was poured over the frozen tissue and a pestle was used to grind and pulverized the sample until a uniformly fine powder was obtained. Pulverized sample was the aliquoted and returned to – 80°C.
Briefly, 500 mL homogenization buffer (Nuclear Isolation Buffer 1 (NIM1) consisting of 250 mM Sucrose, 25 mM KCL, 10 mM Tris-buffer pH 8.0, 5 mM $MgCl_2$, 1 mM DTT, and 10% Triton X-100) were added to powdered tissue and transferred to the mixture a glass Dounce homogenizer and dounced ~ 10 times (avoiding bubbles) on ice. Add homogenization buffer up to 1 mL and filter homogenization solution through a 40 mm cell strainer. Centrifuge filtered solution at 600xg (acceleration 4, deacceleration 4) for 4 min at 4° C. Aspirate supernatant and resuspend in 200 mL of PBS. Nuclei were then count on CellDrop FL (DeNovix) using 1:1 Acridine Orange /Propidium Iodide and homogenization solution. Samples were diluted in PBS to 1 million/mL to seed each well (~30,000 cells in 30 mL/well) of 384 well plate (Perking Elmer PhenoPlate 384-well black, clear flat bottom Cat No. 6057300) pre-coated (1 mL/25 cm^2) with poly-L-Lysine (50 mL/mg). Centrifuge plate at 4000xg for 15 min at 4° C and immediately added 60 mL of 4% PFA to each well and incubate for 15 min at 4° C. Followed by one wash of PBS then proceed with MIEL.

Isolating Peripheral Blood Mononuclear Cells (PBMC's)

200 mL of blood was collected retroorbital for each mouse and immediately mixed with an equal volume of 50 mM EDTA (to prevent coagulation). Blood mixture was further diluted with 200 mL of PBS and carefully layering on top of 750 mL of Ficoll-Paque Plus (Millipore Sigma Cat. No. GE17-1440-02); followed by density gradient centrifugation at 700xg for 30 minutes at room temperature. The PBMC rich layer (cloudy phase) was carefully collected avoiding mixing the above and below layers and transferred to a new tube containing 10 mL of PBS. The PBMC mixture was centrifuged at 700xg for 20 minutes at room temperature and then removed supernatant and resuspend pellet in 1 mL of PBS. Isolated PBMC's were counted manually using a hemocytometer (Hausser Scientific Cat. No. 3120). Samples were diluted in PBS to 1 million/mL to seed each well (~30,000 cells in 30 mL/well) of 384 well plate (Perking Elmer PhenoPlate 384-well black, clear flat bottom Cat No. 6057300) pre-coated (1 mL/25 cm^2) with poly-L-Lysine (50 mL/mg). Centrifuge plate at 4000xg for 15 min at 4° C and immediately added 60 mL of 4% PFA to each well and incubate for 15 min at 4° C followed by PBS wash.

Microscopic Imaging of Epigenetic Landscapes.

Wells were blocked with 2% BSA in PBS 0.5% Triton X-100 for 1 hour at room temperature, and then incubated with primary antibody overnight at 4C and then washed with PBS 3x (5 minutes each at room temperature). Next, wells were incubated with secondary antibody overnight at 4C and then washed with PBS 3x (5 minutes each at room temperature). Antibodies were used at the following concentrations: Anti H3K27ac 1:1000 (Active Motif Cat No. 39685), and /or Anti H3K27me3 1:1000 (Active Motif Cat No. 39155), and/or Anti H3K4me1 1:1000 (Active Motif Cat No. 61633). Antibodies were detected using the following secondary antibodies for their appropriate hots: Goat anti-Rabbit IgG (H+L) Alexa Fluor™ 488 (Thermo Fisher Scientific Cat. No. A11034), and Donkey anti-Mouse IgG (H+L) Alexa Fluor™ 488 (Thermo Fisher Scientific Cat. No. A31570). Wells were counterstained with DAPI (Thermo Fisher Scientific Cat. No. D1306) during the secondary antibody staining and plates were sealed with adhesive foil (VWR Cat. No. 60941-124). Cells/nuclei were imaged on either an Opera Phenix high-content screening system (PerkinElmer) or an IC200-KIC (Vala Sciences) using a 20x objective. At least five fields/well and a total of 9 z-stacks at a 1mm z-step for Opera Phenix and nine fields/well and a total of 10 z-stacks at a 1mm z-step for IC200 were acquired and five wells per mouse sample were imaged. Unless stated otherwise, at least three wells and a minimum of 300 cells for each condition were used for analysis.

Image Segmentation, Feature Extraction and Analysis.
We employed either commercial Acapella 2.6 (PerkinElmer) software package or a custom build python script, which was benchmarked against Acapella software performance. Briefly, DAPI images were used to segment out nuclei generating segmentation masks and object details using either Acapella or StarDist (Schmidt et al, 2018) within a custom python script. Segmentation masks were applied to all channels to isolate raw images of each nucleus in each channel. Size thresholds were then applied to isolate nuclei from debris. Texture features (Threshold Adjacency Statistics) were calculated from each nucleus for each channel as previously described [24]. Bins of 200 nuclei were randomly sampled without replacement per experimental condition. The value for each feature is calculated per bin for the mean statistics. For mean calculations, the features were first normalized via z-scoring. PCA, MDS, and UMAP were calculated from the feature-statistics using the full feature set. Pairwise Euclidean distances were calculated from the feature-statistics. Directionless distance matrix was calculated per data point by averaging the Euclidean distance of that data point to each data point in the reference group. miBioAge distance was calculated as previously described [24].

Hyperbolic embedding
Hyperbolic geometry provides continuous approximation to tree-like hierarchical system, resulting in the distinguishing property of exponential expansion of states compared to quadratic expansion of states in the Euclidean space [81]. The hyperbolic geometry can be visualized using Poincare half space model and Poincare disk [81]. Hyperbolic space is better suited compared to Euclidean space for representing complex multipara metrical biological datasets. This is because hyperbolic space enables using fewer dimensions, inferring the hidden nodes based on the activity of observed "leaf" nodes, and reading out the "centrality" of each node [82-84]. Considering the aging process is due to a sequence of biological changes, and each change is chosen from a variety of choices, hence the number of possible states increase exponentially. We employed the Hyperbolic Multidimensional Scaling (HMDS) [29], which is a version of MDS in the hyperbolic space. Euclidean MDS minimize the difference between the distances calculated in the original Euclidean data space and the distances calculated in the high dimensional reduced space. Once we specify the dimension of the reduced space, the quality of embedding could be assessed using Shepherd diagram, which compares the distance in the original space and the distance in the dimensionality reduced hyperbolic space. The shortest distance between two points in the hyperbolic space is no longer a straight line, but a curved line called geodesic. We define the biological aging axis, analogous to miBioAge in Euclidean space, as the best fitted geodesic for the data of different age in the hyperbolic space. The 3-dimentional hyperbolic embedding was used for the purpose of visualization.

Multidimensional scaling - MDS
The Euclidean distances between all texture feature vectors were calculated to assemble a dissimilarity matrix (size N, where N is the number of populations being compared). For representation, the N matrix was reduced to a Nx2 matrix with MDS using the Excel add-on program XLSTAT (Base, v19.06), and visualized as a 2D scatter plot.

Discriminant Analysis
Quadratic discriminant analysis was conducted using the Excel add-on program XLSTAT (Base, v19.06). The model was generated in a stepwise (forward) approach using default parameters. All features derived from images of tested histone modification were used for analysis following normalization by z-score. Features displaying multicollinearity were reduced. Model training was done as previously described [24].

Doxorubicin treatment

Two months old C57BL/6 mice were intraperitoneal injected with doxorubicin (Santa Cruz Biotechnology, Cat. No. 25316-40-9) 10 mg/Kg. Doxorubicin was diluted in 150mM NaCl solution, and control mice were injected only with the vehicle solution (150mM NaCl). Fourteen days after treatment, mice were sacrificed and liver collected and immediately snap frozen in liquid nitrogen.

Caloric Restriction regimen

Animal studies were conducted in accordance with approved protocols submitted through the respective Institutional Animal Care and Use Committees (IACUCs) at the University of Wisconsin Madison. Caloric Restriction mice: male C57BL/6N mice were individually housed under pathogen free conditions. Mice were randomized into control or restricted groups at 2 months of age and fed the AIN-93M semi-purified diet (Bio-Serv) either a Control diet (95% ad libitum) or Restricted diet (25% less than control). The mice were sacrificed at 7 months of age and tissues were harvested, flash frozen and stored at -80°C.

Acknowledgements.

We greatly appreciate help of Sanford Burnham Prebys animal and high throughput imaging core facilities personnel and leadership in particular Mary O'Rourke-Braxtan and Susanne Heynen-Genel. We thank Collin Kaufman for help with preparing and imaging fresh frozen tissues samples. We thank Kenta Ninomiya and all members of Terskikh laboratory for helpful discussion.

References.

1. Lopez-Otin, C., M.A. Blasco, L. Partridge, M. Serrano, and G. Kroemer, *The hallmarks of aging.* Cell, 2013. **153**(6): p. 1194-217. PMID: 23746838; https://www.ncbi.nlm.nih.gov/pubmed/23746838
2. Pagiatakis, C., E. Musolino, R. Gornati, G. Bernardini, and R. Papait, *Epigenetics of aging and disease: a brief overview.* Aging Clin Exp Res, 2019. PMID: 31811572; https://www.ncbi.nlm.nih.gov/pubmed/31811572
3. Lehnertz, B., Y. Ueda, A.A. Derijck, U. Braunschweig, L. Perez-Burgos, S. Kubicek, T. Chen, E. Li, T. Jenuwein, and A.H. Peters, *Suv39h-mediated histone H3 lysine 9 methylation directs DNA methylation to major satellite repeats at pericentric heterochromatin.* Curr Biol, 2003. **13**(14): p. 1192-200. PMID: 12867029; https://www.ncbi.nlm.nih.gov/pubmed/12867029
4. Wang, Z., C. Zang, J.A. Rosenfeld, D.E. Schones, A. Barski, S. Cuddapah, K. Cui, T.Y. Roh, W. Peng, M.Q. Zhang, and K. Zhao, *Combinatorial patterns of histone acetylations and methylations in the human genome.* Nat Genet, 2008. **40**(7): p. 897-903. PMID: 18552846; http://www.ncbi.nlm.nih.gov/pubmed/18552846
5. Boyer, L.A., K. Plath, J. Zeitlinger, T. Brambrink, L.A. Medeiros, T.I. Lee, S.S. Levine, M. Wernig, A. Tajonar, M.K. Ray, G.W. Bell, A.P. Otte, M. Vidal, D.K. Gifford, R.A. Young, and R. Jaenisch, *Polycomb complexes repress developmental regulators in murine embryonic stem cells.* Nature, 2006. **441**(7091): p. 349-53. PMID: 16625203; https://www.ncbi.nlm.nih.gov/pubmed/16625203
6. van Kruijsbergen, I., S. Hontelez, D.M. Elurbe, S.J. van Heeringen, M.A. Huynen, and G.J.C. Veenstra, *Heterochromatic histone modifications at transposons in Xenopus tropicalis embryos.* Dev Biol, 2017. **426**(2): p. 460-471. PMID: 27639284; https://www.ncbi.nlm.nih.gov/pubmed/27639284
7. Nelson, D.M., F. Jaber-Hijazi, J.J. Cole, N.A. Robertson, J.S. Pawlikowski, K.T. Norris, S.W. Criscione, N.A. Pchelintsev, D. Piscitello, N. Stong, T.S. Rai, T. McBryan, G.L. Otte, C. Nixon, W. Clark, H. Riethman, H. Wu, G. Schotta, B.A. Garcia, N. Neretti, et al., *Mapping H4K20me3 onto the chromatin landscape of senescent cells indicates a function in control of cell senescence and tumor suppression through preservation of genetic and epigenetic stability.* Genome Biol, 2016. **17**(1): p. 158. PMID: 27457071; https://www.ncbi.nlm.nih.gov/pubmed/27457071

8. Creyghton, M.P., A.W. Cheng, G.G. Welstead, T. Kooistra, B.W. Carey, E.J. Steine, J. Hanna, M.A. Lodato, G.M. Frampton, P.A. Sharp, L.A. Boyer, R.A. Young, and R. Jaenisch, *Histone H3K27ac separates active from poised enhancers and predicts developmental state.* Proc Natl Acad Sci U S A, 2010. **107**(50): p. 21931-6. PMID: 21106759; http://www.ncbi.nlm.nih.gov/pubmed/21106759
9. Ucar, D., E.J. Marquez, C.H. Chung, R. Marches, R.J. Rossi, A. Uyar, T.C. Wu, J. George, M.L. Stitzel, A.K. Palucka, G.A. Kuchel, and J. Banchereau, *The chromatin accessibility signature of human immune aging stems from CD8(+) T cells.* J Exp Med, 2017. **214**(10): p. 3123-3144. PMID: 28904110; https://www.ncbi.nlm.nih.gov/pubmed/28904110
10. Maybury-Lewis, S.Y., A.K. Brown, M. Yeary, A. Sloutskin, S. Dhakal, T. Juven-Gershon, and A.E. Webb, *Changing and stable chromatin accessibility supports transcriptional overhaul during neural stem cell activation and is altered with age.* Aging Cell, 2021. **20**(11): p. e13499. PMID: 34687484; https://www.ncbi.nlm.nih.gov/pubmed/34687484
11. Sen, P., P.P. Shah, R. Nativio, and S.L. Berger, *Epigenetic Mechanisms of Longevity and Aging.* Cell, 2016. **166**(4): p. 822-39. PMID: 27518561; https://www.ncbi.nlm.nih.gov/pubmed/27518561
12. Hannum, G., J. Guinney, L. Zhao, L. Zhang, G. Hughes, S. Sadda, B. Klotzle, M. Bibikova, J.B. Fan, Y. Gao, R. Deconde, M. Chen, I. Rajapakse, S. Friend, T. Ideker, and K. Zhang, *Genome-wide methylation profiles reveal quantitative views of human aging rates.* Mol Cell, 2013. **49**(2): p. 359-67. PMID: 23177740; http://www.ncbi.nlm.nih.gov/pubmed/23177740
13. Horvath, S., *DNA methylation age of human tissues and cell types.* Genome Biol, 2013. **14**(10): p. R115. PMID: 24138928; http://www.ncbi.nlm.nih.gov/pubmed/24138928
14. Lowe, R., C. Barton, C.A. Jenkins, C. Ernst, O. Forman, D.S. Fernandez-Twinn, C. Bock, S.J. Rossiter, C.G. Faulkes, S.E. Ozanne, L. Walter, D.T. Odom, C. Mellersh, and V.K. Rakyan, *Ageing-associated DNA methylation dynamics are a molecular readout of lifespan variation among mammalian species.* Genome Biol, 2018. **19**(1): p. 22. PMID: 29452591; https://www.ncbi.nlm.nih.gov/pubmed/29452591
15. Galow, A.M. and S. Peleg, *How to Slow down the Ticking Clock: Age-Associated Epigenetic Alterations and Related Interventions to Extend Life Span.* Cells, 2022. **11**(3). PMID: 35159278; https://www.ncbi.nlm.nih.gov/pubmed/35159278
16. Lu, A.T., A. Quach, J.G. Wilson, A.P. Reiner, A. Aviv, K. Raj, L. Hou, A.A. Baccarelli, Y. Li, J.D. Stewart, E.A. Whitsel, T.L. Assimes, L. Ferrucci, and S. Horvath, *DNA methylation GrimAge strongly predicts lifespan and healthspan.* Aging (Albany NY), 2019. **11**(2): p. 303-327. PMID: 30669119; https://www.ncbi.nlm.nih.gov/pubmed/30669119
17. Weidner, C.I., Q. Lin, C.M. Koch, L. Eisele, F. Beier, P. Ziegler, D.O. Bauerschlag, K.H. Jockel, R. Erbel, T.W. Muhleisen, M. Zenke, T.H. Brummendorf, and W. Wagner, *Aging of blood can be tracked by DNA methylation changes at just three CpG sites.* Genome Biol, 2014. **15**(2): p. R24. PMID: 24490752; https://www.ncbi.nlm.nih.gov/pubmed/24490752
18. Galkin, F., P. Mamoshina, K. Kochetov, D. Sidorenko, and A. Zhavoronkov, *DeepMAge: A Methylation Aging Clock Developed with Deep Learning.* Aging Dis, 2020;
19. Bell, C.G., R. Lowe, P.D. Adams, A.A. Baccarelli, S. Beck, J.T. Bell, B.C. Christensen, V.N. Gladyshev, B.T. Heijmans, S. Horvath, T. Ideker, J.J. Issa, K.T. Kelsey, R.E. Marioni, W. Reik, C.L. Relton, L.C. Schalkwyk, A.E. Teschendorff, W. Wagner, K. Zhang, et al., *DNA methylation aging clocks: challenges and recommendations.* Genome Biol, 2019. **20**(1): p. 249. PMID: 31767039; https://www.ncbi.nlm.nih.gov/pubmed/31767039
20. Jazwinski, S.M. and S. Kim, *Examination of the Dimensions of Biological Age.* Front Genet, 2019. **10**: p. 263. PMID: 30972107; https://www.ncbi.nlm.nih.gov/pubmed/30972107
21. Field, A.E., N.A. Robertson, T. Wang, A. Havas, T. Ideker, and P.D. Adams, *DNA Methylation Clocks in Aging: Categories, Causes, and Consequences.* Molecular Cell, 2018. **71**: p. 882-895;

22. Levine, M.E., A.T. Lu, A. Quach, B.H. Chen, T.L. Assimes, S. Bandinelli, L. Hou, A.A. Baccarelli, J.D. Stewart, Y. Li, E.A. Whitsel, J.G. Wilson, A.P. Reiner, A. Aviv, K. Lohman, Y. Liu, L. Ferrucci, and S. Horvath, *An epigenetic biomarker of aging for lifespan and healthspan.* Aging (Albany NY), 2018. **10**(4): p. 573-591. PMID: 29676998; https://www.ncbi.nlm.nih.gov/pubmed/29676998
23. Zhang, Q., C.L. Vallerga, R.M. Walker, T. Lin, A.K. Henders, G.W. Montgomery, J. He, D. Fan, J. Fowdar, M. Kennedy, T. Pitcher, J. Pearson, G. Halliday, J.B. Kwok, I. Hickie, S. Lewis, T. Anderson, P.A. Silburn, G.D. Mellick, S.E. Harris, et al., *Improved precision of epigenetic clock estimates across tissues and its implication for biological ageing.* Genome Med, 2019. **11**(1): p. 54. PMID: 31443728; https://www.ncbi.nlm.nih.gov/pubmed/31443728
24. Farhy, C., S. Hariharan, J. Ylanko, L. Orozco, F.Y. Zeng, I. Pass, F. Ugarte, E.C. Forsberg, C.T. Huang, D.W. Andrews, and A.V. Terskikh, *Improving drug discovery using image-based multiparametric analysis of the epigenetic landscape.* Elife, 2019. **8**. PMID: 31637999; https://www.ncbi.nlm.nih.gov/pubmed/31637999
25. Severgnini, M., J. Sherman, A. Sehgal, N.K. Jayaprakash, J. Aubin, G. Wang, L. Zhang, C.G. Peng, K. Yucius, J. Butler, and K. Fitzgerald, *A rapid two-step method for isolation of functional primary mouse hepatocytes: cell characterization and asialoglycoprotein receptor based assay development.* Cytotechnology, 2012. **64**(2): p. 187-95. PMID: 22105762; https://www.ncbi.nlm.nih.gov/pubmed/22105762
26. Zhou, Y. and T.O. Sharpee, *Using global t-SNE to preserve inter-cluster data structure.* bioarxiv, 2018;
27. Zhou, Y. and T.O. Sharpee, *Hyperbolic geometry of gene expression.* iScience, 2021. **24**(3): p. 102225. PMID: 33748711; https://www.ncbi.nlm.nih.gov/pubmed/33748711
28. Zhou, Y., B.H. Smith, and T.O. Sharpee, *Hyperbolic geometry of the olfactory space.* Sci Adv, 2018. **4**(8): p. eaaq1458. PMID: 30167457; https://www.ncbi.nlm.nih.gov/pubmed/30167457
29. Praturu, A. and T. Sharpee, *A Bayesian Approach to Hyperbolic Embeddings.* Bulletin of the American Physical Society, 2022;
30. Mager, S.R., M.H. Oomen, M.M. Morente, C. Ratcliffe, K. Knox, D.J. Kerr, F. Pezzella, and P.H. Riegman, *Standard operating procedure for the collection of fresh frozen tissue samples.* Eur J Cancer, 2007. **43**(5): p. 828-34. PMID: 17329097; https://www.ncbi.nlm.nih.gov/pubmed/17329097
31. Naber, S.P., *Continuing role of a frozen-tissue bank in molecular pathology.* Diagn Mol Pathol, 1996. **5**(4): p. 253-9. PMID: 8955616; https://www.ncbi.nlm.nih.gov/pubmed/8955616
32. Shabihkhani, M., G.M. Lucey, B. Wei, S. Mareninov, J.J. Lou, H.V. Vinters, E.J. Singer, T.F. Cloughesy, and W.H. Yong, *The procurement, storage, and quality assurance of frozen blood and tissue biospecimens in pathology, biorepository, and biobank settings.* Clin Biochem, 2014. **47**(4-5): p. 258-66. PMID: 24424103; https://www.ncbi.nlm.nih.gov/pubmed/24424103
33. Demaria, M., M.N. O'Leary, J. Chang, L. Shao, S. Liu, F. Alimirah, K. Koenig, C. Le, N. Mitin, A.M. Deal, S. Alston, E.C. Academia, S. Kilmarx, A. Valdovinos, B. Wang, A. de Bruin, B.K. Kennedy, S. Melov, D. Zhou, N.E. Sharpless, et al., *Cellular Senescence Promotes Adverse Effects of Chemotherapy and Cancer Relapse.* Cancer Discov, 2017. **7**(2): p. 165-176. PMID: 27979832; https://www.ncbi.nlm.nih.gov/pubmed/27979832
34. Baar, M.P., R.M.C. Brandt, D.A. Putavet, J.D.D. Klein, K.W.J. Derks, B.R.M. Bourgeois, S. Stryeck, Y. Rijksen, H. van Willigenburg, D.A. Feijtel, I. van der Pluijm, J. Essers, W.A. van Cappellen, I.W.F. van, A.B. Houtsmuller, J. Pothof, R.W.F. de Bruin, T. Madl, J.H.J. Hoeijmakers, J. Campisi, et al., *Targeted Apoptosis of Senescent Cells Restores Tissue Homeostasis in Response to Chemotoxicity and Aging.* Cell, 2017. **169**(1): p. 132-147 e16. PMID: 28340339; https://www.ncbi.nlm.nih.gov/pubmed/28340339

35. Cupit-Link, M.C., J.L. Kirkland, K.K. Ness, G.T. Armstrong, T. Tchkonia, N.K. LeBrasseur, S.H. Armenian, K.J. Ruddy, and S.K. Hashmi, *Biology of premature ageing in survivors of cancer.* ESMO Open, 2017. **2**(5): p. e000250. PMID: 29326844; https://www.ncbi.nlm.nih.gov/pubmed/29326844
36. Hill, A., J. Sadda, M.A. LaBarge, and A. Hurria, *How cancer therapeutics cause accelerated aging: Insights from the hallmarks of aging.* J Geriatr Oncol, 2020. **11**(2): p. 191-193. PMID: 30905710; https://www.ncbi.nlm.nih.gov/pubmed/30905710
37. Madeo, F., D. Carmona-Gutierrez, S.J. Hofer, and G. Kroemer, *Caloric Restriction Mimetics against Age-Associated Disease: Targets, Mechanisms, and Therapeutic Potential.* Cell Metab, 2019. **29**(3): p. 592-610. PMID: 30840912; https://www.ncbi.nlm.nih.gov/pubmed/30840912
38. Ma, S. and V.N. Gladyshev, *Molecular signatures of longevity: Insights from cross-species comparative studies.* Semin Cell Dev Biol, 2017. **70**: p. 190-203. PMID: 28800931; https://www.ncbi.nlm.nih.gov/pubmed/28800931
39. Balasubramanian, P., P.R. Howell, and R.M. Anderson, *Aging and Caloric Restriction Research: A Biological Perspective With Translational Potential.* EBioMedicine, 2017. **21**: p. 37-44. PMID: 28648985; https://www.ncbi.nlm.nih.gov/pubmed/28648985
40. Lacar, B., S.B. Linker, B.N. Jaeger, S. Krishnaswami, J. Barron, M. Kelder, S. Parylak, A. Paquola, P. Venepally, M. Novotny, C. O'Connor, C. Fitzpatrick, J. Erwin, J.Y. Hsu, D. Husband, M.J. McConnell, R. Lasken, and F.H. Gage, *Nuclear RNA-seq of single neurons reveals molecular signatures of activation.* Nat Commun, 2016. **7**: p. 11022. PMID: 27090946; https://www.ncbi.nlm.nih.gov/pubmed/27090946
41. Nie, C., Y. Li, R. Li, Y. Yan, D. Zhang, T. Li, Z. Li, Y. Sun, H. Zhen, J. Ding, Z. Wan, J. Gong, Y. Shi, Z. Huang, Y. Wu, K. Cai, Y. Zong, Z. Wang, R. Wang, M. Jian, et al., *Distinct biological ages of organs and systems identified from a multi-omics study.* Cell Rep, 2022. **38**(10): p. 110459. PMID: 35263580; https://www.ncbi.nlm.nih.gov/pubmed/35263580
42. Schaum, N., B. Lehallier, O. Hahn, R. Pálovics, S. Hosseinzadeh, S.E. Lee, R. Sit, D.P. Lee, P.M. Losada, M.E. Zardeneta, T. Fehlmann, J.T. Webber, A. McGeever, K. Calcuttawala, H. Zhang, D. Berdnik, V. Mathur, W. Tan, A. Zee, M. Tan, et al., *Ageing hallmarks exhibit organ-specific temporal signatures.* Nature, 2020. **583**(7817): p. 596-602. PMID: 32669715;
43. Carter, T.A., J.A. Greenhall, S. Yoshida, S. Fuchs, R. Helton, A. Swaroop, D.J. Lockhart, and C. Barlow, *Mechanisms of aging in senescence-accelerated mice.* Genome Biol, 2005. **6**(6): p. R48. PMID: 15960800; https://www.ncbi.nlm.nih.gov/pubmed/15960800
44. Ahadi, S., W. Zhou, S.M. Schussler-Fiorenza Rose, M.R. Sailani, K. Contrepois, M. Avina, M. Ashland, A. Brunet, and M. Snyder, *Personal aging markers and ageotypes revealed by deep longitudinal profiling.* Nat Med, 2020. **26**(1): p. 83-90. PMID: 31932806; https://www.ncbi.nlm.nih.gov/pubmed/31932806
45. Cevenini, E., L. Invidia, F. Lescai, S. Salvioli, P. Tieri, G. Castellani, and C. Franceschi, *Human models of aging and longevity.* Expert Opin Biol Ther, 2008. **8**(9): p. 1393-405. PMID: 18694357; https://www.ncbi.nlm.nih.gov/pubmed/18694357
46. Kreienkamp, R., S. Graziano, N. Coll-Bonfill, G. Bedia-Diaz, E. Cybulla, A. Vindigni, D. Dorsett, N. Kubben, L.F.Z. Batista, and S. Gonzalo, *A Cell-Intrinsic Interferon-like Response Links Replication Stress to Cellular Aging Caused by Progerin.* Cell Rep, 2018. **22**(8): p. 2006-2015. PMID: 29466729; https://www.ncbi.nlm.nih.gov/pubmed/29466729
47. Johnson, A.A., K. Akman, S.R. Calimport, D. Wuttke, A. Stolzing, and J.P. de Magalhães, *The role of DNA methylation in aging, rejuvenation, and age-related disease.* Rejuvenation Res, 2012. **15**(5): p. 483-94. PMID: 23098078;
48. Nyce, J., *Drug-induced DNA hypermethylation and drug resistance in human tumors.* Cancer Res, 1989. **49**(21): p. 5829-36. PMID: 2790794;

49. Sun, L., H. Zhang, and P. Gao, *Metabolic reprogramming and epigenetic modifications on the path to cancer.* Protein Cell, 2022. **13**(12): p. 877-919. PMID: 34050894;
50. Ellis, L., P.W. Atadja, and R.W. Johnstone, *Epigenetics in cancer: targeting chromatin modifications.* Mol Cancer Ther, 2009. **8**(6): p. 1409-20. PMID: 19509247;
51. Herranz, M. and M. Esteller, *DNA methylation and histone modifications in patients with cancer: potential prognostic and therapeutic targets.* Methods Mol Biol, 2007. **361**: p. 25-62. PMID: 17172706;
52. Schumacher, B., G.A. Garinis, and J.H. Hoeijmakers, *Age to survive: DNA damage and aging.* Trends Genet, 2008. **24**(2): p. 77-85. PMID: 18192065;
53. Hoeijmakers, J.H., *DNA damage, aging, and cancer.* New England Journal of Medicine, 2009. **361**(15): p. 1475-1485;
54. Bohr, V.A. and R.M. Anson, *DNA damage, mutation and fine structure DNA repair in aging.* Mutat Res, 1995. **338**(1-6): p. 25-34. PMID: 7565878;
55. Wang, S., A. Prizment, B. Thyagarajan, and A. Blaes, *Cancer Treatment-Induced Accelerated Aging in Cancer Survivors: Biology and Assessment.* Cancers (Basel), 2021. **13**(3). PMID: 33498754; https://www.ncbi.nlm.nih.gov/pubmed/33498754
56. Shafqat, S., E. Arana Chicas, A. Shafqat, and S.K. Hashmi, *The Achilles' heel of cancer survivors: fundamentals of accelerated cellular senescence.* J Clin Invest, 2022. **132**(13). PMID: 35775492;
57. Guida, J.L., T.A. Ahles, D. Belsky, J. Campisi, H.J. Cohen, J. DeGregori, R. Fuldner, L. Ferrucci, L. Gallicchio, L. Gavrilov, N. Gavrilova, P.A. Green, C. Jhappan, R. Kohanski, K. Krull, J. Mandelblatt, K.K. Ness, A. O'Mara, N. Price, J. Schrack, et al., *Measuring Aging and Identifying Aging Phenotypes in Cancer Survivors.* J Natl Cancer Inst, 2019. **111**(12): p. 1245-1254. PMID: 31321426;
58. Olsen, J.H., T. Moller, H. Anderson, F. Langmark, R. Sankila, L. Tryggvadottir, J.F. Winther, C. Rechnitzer, G. Jonmundsson, J. Christensen, and S. Garwicz, *Lifelong cancer incidence in 47,697 patients treated for childhood cancer in the Nordic countries.* J Natl Cancer Inst, 2009. **101**(11): p. 806-13. PMID: 19470947; https://www.ncbi.nlm.nih.gov/pubmed/19470947
59. Rebholz, C.E., R.C. Reulen, A.A. Toogood, C. Frobisher, E.R. Lancashire, D.L. Winter, C.E. Kuehni, and M.M. Hawkins, *Health care use of long-term survivors of childhood cancer: the British Childhood Cancer Survivor Study.* J Clin Oncol, 2011. **29**(31): p. 4181-8. PMID: 21947833; https://www.ncbi.nlm.nih.gov/pubmed/21947833
60. Soto-Perez-de-Celis, E., D. Li, Y. Yuan, Y.M. Lau, and A. Hurria, *Functional versus chronological age: geriatric assessments to guide decision making in older patients with cancer.* Lancet Oncol, 2018. **19**(6): p. e305-e316. PMID: 29893262; https://www.ncbi.nlm.nih.gov/pubmed/29893262
61. Bhakta, N., Q. Liu, F. Yeo, M. Baassiri, M.J. Ehrhardt, D.K. Srivastava, M.L. Metzger, M.J. Krasin, K.K. Ness, M.M. Hudson, Y. Yasui, and L.L. Robison, *Cumulative burden of cardiovascular morbidity in paediatric, adolescent, and young adult survivors of Hodgkin's lymphoma: an analysis from the St Jude Lifetime Cohort Study.* Lancet Oncol, 2016. **17**(9): p. 1325-34. PMID: 27470081;
62. Peter, S., S. Alven, R.B. Maseko, and B.A. Aderibigbe, *Doxorubicin-Based Hybrid Compounds as Potential Anticancer Agents: A Review.* Molecules, 2022. **27**(14). PMID: 35889350;
63. Geisberg, C.A. and D.B. Sawyer, *Mechanisms of anthracycline cardiotoxicity and strategies to decrease cardiac damage.* Curr Hypertens Rep, 2010. **12**(6): p. 404-10. PMID: 20842465;
64. Bullard, B.M., S.J. McDonald, T.D. Cardaci, B.N. VanderVeen, and E.A. Murphy, *Nonpharmacological approaches for improving gut resilience to chemotherapy.* Current Opinion in Supportive and Palliative Care, 2022. **16**(3): p. 151-160;
65. Liao, C.Y., B.A. Rikke, T.E. Johnson, V. Diaz, and J.F. Nelson, *Genetic variation in the murine lifespan response to dietary restriction: from life extension to life shortening.* Aging Cell, 2010. **9**(1): p. 92-5. PMID: 19878144; https://www.ncbi.nlm.nih.gov/pubmed/19878144

66. Harper, J.M., C.W. Leathers, and S.N. Austad, *Does caloric restriction extend life in wild mice?* Aging Cell, 2006. **5**(6): p. 441-9. PMID: 17054664; https://www.ncbi.nlm.nih.gov/pubmed/17054664
67. Heilbronn, L.K. and E. Ravussin, *Calorie restriction and aging: review of the literature and implications for studies in humans.* Am J Clin Nutr, 2003. **78**(3): p. 361-9. PMID: 12936916; https://www.ncbi.nlm.nih.gov/pubmed/12936916
68. Al-Regaiey, K.A., *The effects of calorie restriction on aging: a brief review.* Eur Rev Med Pharmacol Sci, 2016. **20**(11): p. 2468-73. PMID: 27338076; https://www.ncbi.nlm.nih.gov/pubmed/27338076
69. Liang, Y., C. Liu, M. Lu, Q. Dong, Z. Wang, Z. Wang, W. Xiong, N. Zhang, J. Zhou, Q. Liu, X. Wang, and Z. Wang, *Calorie restriction is the most reasonable anti-ageing intervention: a meta-analysis of survival curves.* Sci Rep, 2018. **8**(1): p. 5779. PMID: 29636552; https://www.ncbi.nlm.nih.gov/pubmed/29636552
70. Policarpi, C., M. Munafo, S. Tsagkris, V. Carlini, and J.A. Hackett, *Systematic Epigenome Editing Captures the Context-dependent Instructive Function of Chromatin Modifications.* bioRxiv, 2022;
71. Grewal, S.I. and D. Moazed, *Heterochromatin and epigenetic control of gene expression.* Science, 2003. **301**(5634): p. 798-802. PMID: 12907790; https://www.ncbi.nlm.nih.gov/pubmed/12907790
72. Baker, M., *Making sense of chromatin states.* Nat Methods, 2011. **8**(9): p. 717-22. PMID: 21878916; https://www.ncbi.nlm.nih.gov/pubmed/21878916
73. Heintzman, N.D., G.C. Hon, R.D. Hawkins, P. Kheradpour, A. Stark, L.F. Harp, Z. Ye, L.K. Lee, R.K. Stuart, C.W. Ching, K.A. Ching, J.E. Antosiewicz-Bourget, H. Liu, X. Zhang, R.D. Green, V.V. Lobanenkov, R. Stewart, J.A. Thomson, G.E. Crawford, M. Kellis, et al., *Histone modifications at human enhancers reflect global cell-type-specific gene expression.* Nature, 2009. **459**(7243): p. 108-12. PMID: 19295514; http://www.ncbi.nlm.nih.gov/entrez/query.fcgi?cmd=Retrieve&db=PubMed&dopt=Citation&list_uids=19295514
74. Rye, M., P. Sætrom, T. Håndstad, and F. Drabløs, *Clustered ChIP-Seq-defined transcription factor binding sites and histone modifications map distinct classes of regulatory elements.* BMC Biol, 2011. **9**: p. 80. PMID: 22115494;
75. Strahl, B.D. and C.D. Allis, *The language of covalent histone modifications.* Nature, 2000. **403**(6765): p. 41-5. PMID: 10638745; https://www.ncbi.nlm.nih.gov/pubmed/10638745
76. Fraga, M.F. and M. Esteller, *Epigenetics and aging: the targets and the marks.* Trends Genet, 2007. **23**(8): p. 413-8. PMID: 17559965; https://www.ncbi.nlm.nih.gov/pubmed/17559965
77. Horvath, S. and K. Raj, *DNA methylation-based biomarkers and the epigenetic clock theory of ageing.* Nat Rev Genet, 2018. **19**(6): p. 371-384. PMID: 29643443; https://www.ncbi.nlm.nih.gov/pubmed/29643443
78. Rakyan, V.K., T.A. Down, S. Maslau, T. Andrew, T.P. Yang, H. Beyan, P. Whittaker, O.T. McCann, S. Finer, A.M. Valdes, R.D. Leslie, P. Deloukas, and T.D. Spector, *Human aging-associated DNA hypermethylation occurs preferentially at bivalent chromatin domains.* Genome Res, 2010. **20**(4): p. 434-9. PMID: 20219945; https://www.ncbi.nlm.nih.gov/pubmed/20219945
79. Wang, T., B. Tsui, J.F. Kreisberg, N.A. Robertson, A.M. Gross, M.K. Yu, H. Carter, H.M. Brown-Borg, P.D. Adams, and T. Ideker, *Epigenetic aging signatures in mice livers are slowed by dwarfism, calorie restriction and rapamycin treatment.* Genome Biol, 2017. **18**(1): p. 57. PMID: 28351423; https://www.ncbi.nlm.nih.gov/pubmed/28351423
https://www.ncbi.nlm.nih.gov/pmc/articles/PMC5371228/pdf/13059_2017_Article_1186.pdf
80. Liu, Z., D. Leung, K. Thrush, W. Zhao, S. Ratliff, T. Tanaka, L.L. Schmitz, J.A. Smith, L. Ferrucci, and M.E. Levine, *Underlying features of epigenetic aging clocks in vivo and in vitro.* Aging Cell, 2020. **19**(10): p. e13229. PMID: 32930491; https://www.ncbi.nlm.nih.gov/pubmed/32930491

81. Sharpee, T.O., *An argument for hyperbolic geometry in neural circuits.* Current opinion in neurobiology, 2019. **58**: p. 101-104;
82. Verleysen, M. and D. François. *The curse of dimensionality in data mining and time series prediction.* in *International work-conference on artificial neural networks*. 2005. Springer.
83. Kuo, F.Y. and I.H. Sloan, *Lifting the curse of dimensionality.* Notices of the AMS, 2005. **52**(11): p. 1320-1328;
84. Bellman, R., *Dynamic programming, 1957.* A very comprehensive reference with many economic examples is, 2003;